Thermal Science and Engineering (2023) Volume 6 Issue 1
doi:10.24294/tse.v6i1.2052

ORIGINAL RESEARCH ARTICLE

Study of surface thermodynamic properties of some boron compounds by inverse gas chromatography at infinite dilution

Tayssir Hamieh[1,2]

[1] *Faculty of Science and Engineering, Maastricht University, 6200 MD Maastricht, Netherlands. E-mail: t.hamieh@maastrichtuniversity.nl*

[2] *Laboratory of Materials, Catalysis, Environment and Analytical Methods Laboratory (MCEMA), Faculty of Sciences, Lebanese University, 1533 Hadath, Lebanon.*

ABSTRACT

This paper is devoted to the determination of the dispersive component of the surface energy of two boron materials such as h-BN and BPO_4 surfaces by using the inverse gas chromatography (IGC) at infinite dilution. The specific interactions and Lewis's acid-base parameters of these materials were calculated on the light of the new thermal model concerning the dependency of the surface area of organic molecules on the temperature, and by using also the classical methods of the inverse gas chromatography as well as the different molecular models such as Van der Waals, Redlich-Kwong, Kiselev, geometric, Gray, spherical, cylindrical and Hamieh models. It was proved that h-BN surface exhibits higher dispersive surface energy than BPO_4 material.

The specific properties of interaction of the two boron materials were determined. The results obtained by using the new thermal model taking into account the effect of the temperature on the surface area of molecules, proved that the classical IGC methods, gave inaccurate values of the specific parameters and Lewis's acid base constants of the solid surfaces. The use of the thermal model allowed to conclude that h-BN surface has a Lewis basicity twice stronger than its acidity, whereas, BPO_4 surface presents an amphoteric character.

Keywords: Retention Volume; Free Surface Energy of Adsorption; Specific Interactions; Lewis's Acid Base Parameters; Hamieh Thermal Effect

ARTICLE INFO

Received: 24 April, 2023
Accepted: 25 June, 2023
Available online: 25 July, 2023

1. Introduction

One of the most famous techniques that give information on the surface properties of materials and nanomaterials is inverse gas chromatography (IGC) at infinite dilution[1]. This technique had a large success to determine the surface physicochemical properties of materials such as the dispersive surface energy γ_s^d, the specific free energy of adsorption ΔG_a^0 and the Lewis-acid base parameters K_A and K_A[2–11].

It is crucial to determine the surface and interface thermodynamic properties of solid materials in many industrial processes such as synthesis, catalysis, photocatalysis, surfactant formulation, chemical engineering, adhesion, adsorption and membrane fabrication. The inverse gas chromatography is the best technique that allows to characterize the physicochemical properties, the dispersive energy and the Lewis acid-base parameters of metals, oxides, clays[9–13], ceramic materials, polymers and composites, textiles, fibers and nanomaterials, pharmaceutical and food products[12–22] and polymers adsorbed on oxides[23–26]. This interesting chromatographic technique is always used to determine the dispersive component of the surface energy, the dispersive and specific free energy of interaction ΔG_a^{sp}, the specific enthalpy ΔH_a^{sp} and

entropy ΔS_a^{sp} of polar molecules adsorbed on the solid surfaces. The Lewis acid base character[3,4,7–10,23–26] can be also determined by IGC at infinite dilution that can quantify the dispersive and polar interactions between materials and nanomaterials and the organic probes generally used in this technique.

In many previous papers[23–29], we used IGC technique to determine the surface and interface properties of some metals, oxides, textiles, polymers adsorbed on oxides and supported catalysts. Some new models and methods were recently proposed in literature[30–33] to correct some incoherencies committed by various scientists[34–40] in order to better understand the behaviour of materials when they are in contact with other materials.

In this paper, we were interested to study the thermodynamic properties of two boron compounds such hexagonal boron nitride (h-BN) and boron phosphate (BPO_4), correct various errors committed by a recent study[39] and thus give more accurate results.

2. Methods

To do that, many methods were proposed in literature and used during the last sixty years[1–33]. At the beginning, Sawyer and Brookman[2] found an excellent linearity of the logarithm of the net retention volume Vn of an adsorbed solvent on a solid, as a function of the boiling point $T_{B.P.}$ of n-alkanes $lnVn = f(T_{B.P.})$. The separation method of the dispersive (or London) and polar (or specific) interactions between a solid substrate and a polar molecule was proposed by the research works of Saint-Flour and Papirer[3,4]. These authors used the representation of $RTlnVn$ versus the logarithm of the vapor pressure P_0 of probes:

$$RTlnVn = \alpha_1 P_0 + \beta_1 \tag{1}$$

where R is the ideal gas constant, T is the absolute temperature and α_1 and β_1 constants depending on the interface solid-solvent. The distance relating the representative point of $RTlnVn$ of a polar molecule to its hypothetic point located on the n-alkane straight-line determined the specific free energy of adsorption ΔG_a^{sp}. The variation of ΔG_a^{sp} versus the temperature led to the specific enthalpy ΔH_a^{sp} and entropy ΔS_a^{sp} of polar molecule adsorbed and therefore to the Lewis acid-base parameters. Several other IGC methods were proposed, to characterize the solid surfaces, a similar linearity to separate the two dispersive and polar components of the specific interactions was found.

On the other hand, two similar methods were used to determine the dispersive component γ_s^d of the surface energy of the solid.

1) Dorris and Gray[41] first determined γ_s^d of solid materials by using Fowkes relation[42] and correlating the work of adhesion W_a to the free energy of adsorption ΔG_a^0 by the following relation:

$$\Delta G_a^0 = \mathcal{N} a\, W_a = 2\mathcal{N} a \sqrt{\gamma_l^d \gamma_s^d} \tag{2}$$

where a is the surface area of adsorbed molecule, γ_l^d is the dispersive component of the liquid solvent, and $\mathcal{N}$ is the Avogadro's number.

Dorris and Gray introduced the increment ΔG^0_{-CH2-} of two consecutive n-alkanes $C_nH_{2(n+1)}$ and $C_nH_{2(n+1)}$:

$$\Delta G^0_{-CH2-} = \Delta G^0\left(C_{n+1}H_{2(n+2)}\right) - \Delta G^0\left(C_nH_{2(n+1)}\right) \tag{3'}$$

By supposing the surface area of methylene group, $a_{-CH2-} = 6$Å, independent from the temperature and the surface energy $\gamma_{-CH2-}(\text{in mJ/m}^2)$ of –CH2– equal to:

$$\gamma_{-CH2-} = 52.603 - 0.058\,T\ (T\ in\ K)$$

Dorris and Gray[41] then deduced the value of γ_s^d by the Equation (3):

$$\gamma_s^d = \frac{\left[RTln\left[\frac{V_n\left(C_{n+1}H_{2(n+2)}\right)}{V_n\left(C_nH_{2(n+1)}\right)}\right]\right]^2}{4\mathcal{N}^2\, a^2_{-CH2-}\gamma_{-CH2-}} \tag{3}$$

2) The method proposed by Schultz *et al.*[5] using Fowkes relation[42] similarly gave the free energy of adsorption ΔG_a^0 as a function of the geometric mean of the respective dispersive components of the surface energy of the liquid solvent γ_l^d and the solid γ_s^d:

$$\Delta G_a^0 = RTlnVn + \alpha_2 = 2\mathcal{N} a \left(\gamma_l^d \gamma_s^d\right)^{1/2} + \beta_2 \tag{4}$$

where a is the surface area of probes supposed constant for all temperatures and α_2 and β_2 two

constants depending on the used materials and the temperature. The variations of $RTlnVn$ versus $2\mathcal{N}a\left(\gamma_l^d\right)^{1/2}$ of n-alkanes and polar molecules gave both the γ_s^d and $\Delta G_a^{sp}(T)$ of the solid.

In previous studies, one determined the dispersive component of many solid materials by using the various molecular areas of Kiselev, Van der Waals (VDW), Redlich-Kwong (R-K), Kiselev, geometric, cylindrical or spherical models[23–26].

3) The method deduced from the works of Sawyer and Brookman[2] used:

$$RTlnVn = \alpha_3 T_{B.P.} + \beta_3 \quad (5)$$

where α_3 and β_3 are two constants. This method gave the specific free energy and the acid base properties.

4) The method of the deformation polarizability α_0 proposed by Donnet *et al.*[43]. They proposed the following relation:

$$RTlnVn = \alpha_4 (h\nu_L)^{1/2}\, \alpha_{0,L} + \beta_4 \quad (6)$$

where ν_L is the electronic frequency of the probe, h is the Planck's constant and α_4 and β_4 are constants of interaction.

5) Chehimi *et al.*[44] used the standard enthalpy of vaporization $\Delta H^0_{vap.}$ (supposed constant) of n-alkanes and polar molecules:

$$RTlnVn = \alpha_5 \Delta H^0_{vap.} + \beta_5 \quad (7)$$

where α_5 and β_5 are two constants. This method is similar to Saint-Flour and Papirer method using lnP_0 and that of Sawyer and Brookman using $T_{B.P.}$.

6) The method of Brendlé and Papirer[14,45] used the concept of the topological index χ_T that is a parameter considering the topology and the local electronic density in the polar probe structure. They gave the following relation:

$$RTlnVn = \alpha_6 f(\chi_T) + \beta_6 \quad (8)$$

where α_6 and β_6 are two adsorption constants.

In all previous cases, the determination of $\Delta G_a^{sp}(T)$ of polar solvents versus the temperature will allow to deduce the specific enthalpy $\left(-\Delta H_a^{sp}\right)$ and entropy $\left(\Delta S_a^{sp}\right)$ of polar probes adsorbed on the solid surfaces by using Equation (1):

$$\Delta G_a^{sp}(T) = \Delta H_a^{sp} - T\,\Delta S_a^{sp} \quad (9)$$

Knowing of ΔH_a^{sp} polar solvents, the two respective acid base constants K_A and K_D of solids can be determined by Papirer following relation[3,4,46]:

$$\frac{-\Delta H^{Sp}}{AN} = \frac{DN}{AN} K_A + K_D \quad (10)$$

where AN and DN respectively represent the electron donor and acceptor numbers of the polar molecule given by Gutmann[47] and corrected by Fowkes.

Criticism of the two methods of Schultz and Dorris-Gray

In previous works[30–33], one proved that the method of Schultz *et al.*[5] cannot be used to characterize the solid surfaces and obtain quantitative properties, because they supposed the surface area of probes as constant and independent from the temperature. While, it was proved that the surface area of molecules is function of the temperature[30–33]. Consequently, the values of γ_s^d, ΔG_a^{sp} and the Lewis acid base parameters obtained many authors are definitely inaccurate and they have to be corrected.

Indeed, Hamieh *et al.*[30] gave the different relations of the surface area $a(T)$ of organic molecules and n-alkanes versus the temperature and the surface area of methylene group $a_{-CH2-}(T)$ also proving the non-validity of γ_s^d determined by Dorris-Gray relation.

Consequently, the values of the dispersive surface energy and the specific interactions of solid materials by using Dorris-Gray and Schultz method are certainly inaccurate. Recently, Isik *et al.*[40] used the above methods to determine the surface properties of boron compounds. Their results are not accurate. A correction has to be introduced to obtain more accurate results.

The values obtained by Isik *et al.*[40] for the hexagonal boron nitride and the boron phosphate were recorrected by our thermal model taking into account the variations of the surface areas of organic molecules as a function of the temperature. We also used all other known IGC methods and models in order to show the large disparity between the obtained values of γ_s^d, ΔG_a^{sp} and the Lewis acid base constants of the two studied materials.

3. Experimental

3.1. Materials and solvents

All chemicals used in this study such as hexagonal boron nitride and boron phosphate, the n-alkanes (hexane, heptane, octane, and nonane), and the polar solvents (strong acid probes (chloroform ($CHCl_3$) and dichloromethane (DCM)), amphoteric solvent (acetone) and strong basic solvents (ethyl acetate and tetrahydrofuran (THF)) at highly pure grade (99%), were purchased from Fisher Scientific.

The above polar organic probes are characterized by their donor and acceptor numbers. The corrected acceptor number and normalized donor number were used in this study and given in **Table 1**.

Table 1. Normalized donor and acceptor numbers of some polar molecules.

Polar probe	DN'	AN'	DN'/AN'	Character
$CHCl_3$	0	18.7	0.00	Higher acidity
CH_2Cl_2	3	13.5	0.22	Acid
Acetone	42.5	8.7	4.89	Higher amphoteric
Ethyl acetate	42.75	5.3	8.07	Base
THF	50	1.9	26.32	Higher basicity

3.2. GC Conditions

The experimental measurements were performed on a commercial Focus GC gas chromatograph equipped with a flame ionization detector. Dried nitrogen was the carrier gas. The gas flow rate was set at 30 mL/min. The injector and detector temperatures were maintained at 400 K during the experiments. To achieve infinite dilution, 0.1 µL of each probe vapor was injected with 1 µL Hamilton syringes, in order to approach linear condition gas chromatography. The two columns used in this study were prepared using a stainless-steel column with a 2 mm inner diameter and with an approximate length of 20 cm. The column was packed with 1 g of solids in powder forms. The column temperatures were between 300 K and 330 K, varied in 5 ºC steps. Each probe injection was repeated three times, and the average retention time, t_R, was used for the calculation. The standard deviation was less than 1% in all measurements.

3.3. Results

3.3.1. Study of the dispersive component of the surface energy

The dispersive components of the surface energy of hexagonal boron nitride and boron phosphate were determined by using Dorris-Gray method, the molecular models and the thermal model[23–26,30–33] taking into account the variations of the surface area versus the temperature.

We plotted on **Figure 1**, the calculated values of $\gamma_s^d(T)$ of hexagonal boron nitride and boron phosphate surfaces versus the temperature by using the above methods. All models and IGC methods gave linear variations with excellent correlation coefficient with decrease of $\gamma_s^d(T)$ of the two materials when the temperature increases. However, we can distinguish here the large difference between the values of $\gamma_s^d(T)$ obtained by the various models and methods proving the non-universality of any of the used methods. The only result that can be considered as more accurate is that base on the thermal model given by Hamieh model[30–33]. **Figure 1** also showed that VDW model gave closer results, but there is a difference between the $\gamma_s^d(T)$ values obtained by Isik *et al.*[40] using the methods of Schultz *et al.*[5] and Dorris-Gray, and that of the thermal model that we applied. The hypothesis of the classic methods of Schultz and Dorris-Gray considering the surface areas of organic molecules as constant independent from the temperature, is wrong. The error exceeds 30% with respect of Hamieh model[30–33]. All methods that do not take into account the thermal effect cannot be considered as qualitative methods but only qualitative and can be used for the comparison between materials. These methods cannot be used for other calculations either, such as the determination of the specific and acid base properties of materials due to this incoherency. The different molecular methods were used to show that there is no raison to limit the calculations only to Kiselev values. Indeed, the gas molecules can have different position during the adsorption or desorption processes and therefore the geometry of molecules can change from model

to another model. For example, the values of the surface area obtained by using Van der Waals equations took into consideration the lateral interactions of molecules where the spherical model supposed the n-alkanes contained in a sphere with a mean value of the radius. Whereas, the cylindrical model supposed a cylindrical geometry of molecules. Only the geometric model gave the real value of the surface area of the molecule by taking its real geometric form[33].

Consequently, we cannot use these above models without considering the effect of the temperature on the surface area of n-alkanes and polar molecules.

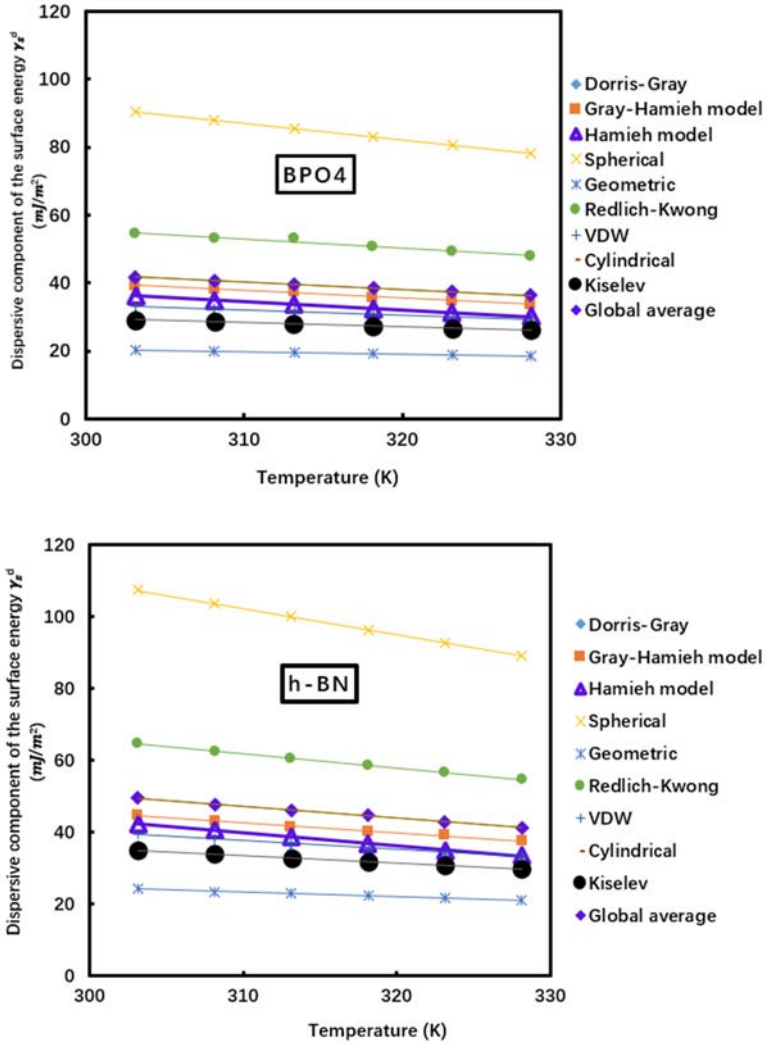

Figure 1. Evolution of γ_s^d (mJ/m^2) of h-BN and BPO_4 as a function of the temperature T (K) for the different methods and models of IGC.

We gave on **Table 2** the equations giving $\gamma_s^d(T)$ of the two boron materials against the temperature by using the different molecular models, the dispersive surface entropy ε_s^d, the extrapolated values $\gamma_s^d(T=0K)$ and the maximum of temperature T_{Max} defined by: $T_{Max} = -\frac{\gamma_s^d(T=0K)}{\varepsilon_s^d}$.

Figure 1 and **Table 2** proved that the dispersive surface energy of h-BN is clearly larger than that of BPO_4. One observed that the results obtained with Redlich-Kwong model is closer to that of Hamieh model once proving the strong effect of the temperature on the surface areas of molecules and therefore on the dispersive surface energy of materials. **Table 2** also showed certain differences in the values of T_{Max} obtained by the various models. However, one observed comparable value of T_{Max} of the two materials by Hamieh model $T_{Max} \approx 420$ K.

On the other hand, **Table 2** showed a difference in the values of $\gamma_s^d(T)$ of h-BN and BPO_4 particles obtained by Hamieh model when comparing with those obtained by Isik *et al.*[40]. Indeed, these authors applied the two methods of Gray and Schultz (using Kiselev results). This difference is due to the fact that the authors neglected the effect of the temperature on the surface areas of organic molecules.

Table 2. Equations $\gamma_s^d(T)$ of h-BN and BPO4 particles for all used molecular models of n-alkanes, ε_s^d, $\gamma_s^d(T=0K)$ and T_{Max}.

Case of BPO_4				
Molecular model	$\gamma_s^d(T)$ **(mJ/m²)**	$\varepsilon_s^d = d\gamma_s^d/dT$ **(mJ m⁻² K⁻¹)**	$\gamma_s^d(T=0K)$ **(mJ/m²)**	T_{Max}
Dorris-Gray	$\gamma_s^d(T) = -0.11T + 65.4$	−0.11	65.4	569.3
Hamieh-Gray	$\gamma_s^d(T) = -0.42T + 187$	−0.42	187.0	441.0
Hamieh model	$\gamma_s^d(T) = -0.44T + 183.7$	−0.44	183.7	416.1
Spherical	$\gamma_s^d(T) = -0.49T + 239.8$	−0.49	239.8	487.3
Geometric	$\gamma_s^d(T) = -0.07T + 41.7$	−0.07	41.7	588.7
Redlich-Kwong	$\gamma_s^d(T) = -0.22T + 137.2$	−0.22	137.2	631.7
VDW	$\gamma_s^d(T) = -0.16T + 82.1$	−0.16	82.1	509.2
Cylindrical	$\gamma_s^d(T) = -0.11T + 61.9$	−0.11	61.9	548.6
Kiselev	$\gamma_s^d(T) = -0.13T + 68.3$	−0.13	68.3	529.3
Global average	$\gamma_s^d(T) = -0.24T + 116.4$	−0.24	116.4	485.0
Case of h-BN				
Molecular model	$\gamma_s^d(T)$ **(mJ/m²)**	$\varepsilon_s^d = d\gamma_s^d/dT$ **(mJ m⁻² K⁻¹)**	$\gamma_s^d(T=0K)$ **(mJ/m²)**	T_{Max}
Dorris-Gray	$\gamma_s^d(T) = -0.15T + 80.8$	−0.15	80.8	547.0
Hamieh-Gray	$\gamma_s^d(T) = -0.28T + 130.7$	−0.28	130.7	459.9
Hamieh model	$\gamma_s^d(T) = -0.36T + 152$	−0.36	152.0	419.9
Spherical	$\gamma_s^d(T) = -0.73T + 328.6$	−0.73	328.6	450.0
Geometric	$\gamma_s^d(T) = -0.12T + 60.7$	−0.12	60.7	502.7
Redlich-Kwong	$\gamma_s^d(T) = -0.40T + 185.6$	−0.40	185.6	464.7
VDW	$\gamma_s^d(T) = -0.24T + 112.8$	−0.24	112.8	464.9
Cylindrical	$\gamma_s^d(T) = -0.18T + 88.2$	−0.18	88.2	483.6
Kiselev	$\gamma_s^d(T) = -0.21T + 97.0$	−0.21	97.0	472.2
Global average	$\gamma_s^d(T) = -0.32T + 146.4$	−0.32	146.4	457.0

Due to the large disparities in the γ_s^d values between the different models. We will determine the specific or polar properties of materials by using the different methods in order to prove the no-validity of Schultz *et al*. method[5] and therefore this method cannot be used for the determination of the specific and acid base properties of materials.

3.3.2. Specific free energy ($\Delta G_a^{sp}(T)$) and acid-base constants of materials

In this section, one used the nine molecular models including the thermal model with the vapor pressure[3,4], deformation polarizability[43], topological index, boiling point[2] and vaporization heat[44] methods, to determine the values of the specific free energy ($\Delta G_a^{sp}(T)$) of the different polar solvents adsorbed on BPO_4 and h-BN surfaces as a function of the temperature (See **Tables A1** and **A2** in Appendix). All used methods and models gave linear relations of ($\Delta G_a^{sp}(T)$) but one also observed irregular results between the various IGC methods and models.

The large difference between the ($\Delta G_a^{sp}(T)$) values obtained with h-BN and BPO_4 can be shown on **Figure 2**. That clearly proved that the values of the specific free energy of an adsorbed solvent can be 3 or 4 times higher from an applied model to another model. The study of the specific free energy of the different solvents such as $CHCl_3$, CH_2Cl_2, THF, Ethyl acetate and acetone adsorbed on the boron compounds revealed a large difference between the values obtained the different IGC models and methods. For example, in the case of $CHCl_3$ and CH_2Cl_2, we observed that the values of ΔG_a^{sp} varies from 1 kJ/mol to 9 kJ/mol. The same irregularities were observed with tho other solvents, proving the necessity to the correction of the classical methods by the use of the thermal model taking into account the effect of the temperature on the surface area of organic molecules.

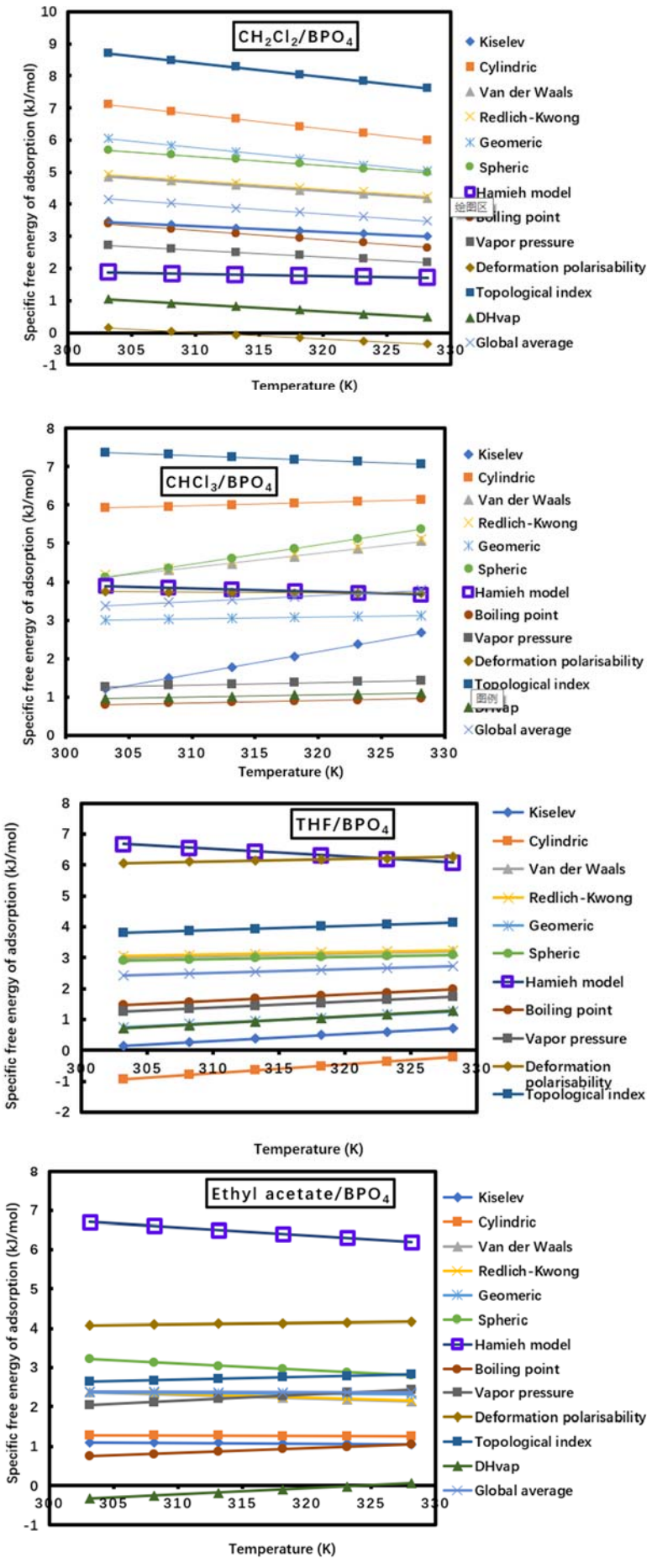

Figure 2. (*Continued*).

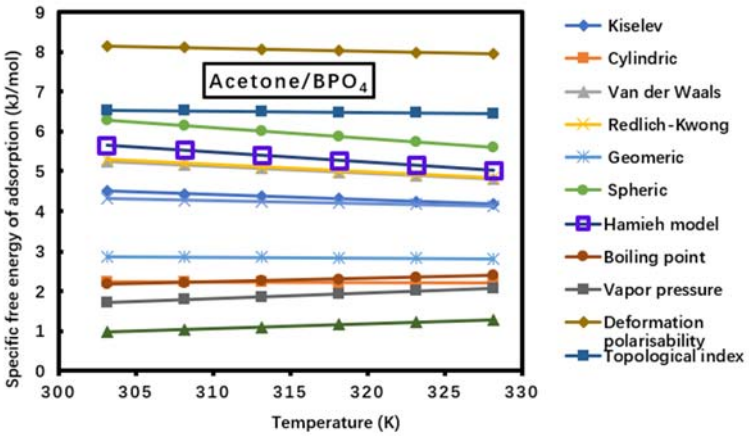

Figure 2. Variations of ΔG_a^{sp} of the various solvents ($CHCl_3$, CH_2Cl_2, THF, Ethyl acetate and acetone) adsorbed on BPO_4 as a function of the temperature for the different IGC models and methods.

Now to determine the specific enthalpy and entropy of adsorption of polar molecules on the solid surfaces, one used the above values of $\Delta G_a^{sp}(T)$ obtained by the different methods and relation (9).

3.3.3. Enthalpic and entropic acid base constants

By using relation (9) and $\Delta G_a^{sp}(T)$ values, one deuced $(-\Delta H_a^{sp})$ and $(-\Delta S_a^{sp})$ of the different polar solvents adsorbed on BPO_4 and h-BN surfaces for the different used methods (**Tables 3** and **4**).

One found that there was a large difference between the different values of $(-\Delta H_a^{sp})$ (**Table 3**) and $(-\Delta S_a^{sp})$ (**Table 4**) of dichloromethane, chloroform, THF, ethyl acetate and acetone adsorbed on materials strongly depending on the used molecular model or IGC method. Only the thermal model gave more accurate results because it took into account the thermal effect of the temperature on the surface area.

Table 3. Variations of $(-\Delta H_a^{sp}\ in\ kJ\ mol^{-1})$ as a function of the used models or methods of the adsorbed polar molecules respectively on BPO_4 and h-BN materials.

BPO_4 surface					
Model or method	**CH_2Cl_2**	**Chloroform**	**THF**	**Ethyl acetate**	**Acetone**
Kiselev	41.026	28.691	35.500	23.517	24.226
Cylindric	20.705	3.301	−9.342	1.549	2.731
Van der Waals	12.878	−7.186	0.709	5.065	10.867
Redlich-Kwong	13.077	−7.051	0.854	5.172	10.997
Geomeric	18.493	1.857	5.431	3.042	3.486
Spheric	14.187	11.115	0.807	8.133	14.405
Hamieh model	4.000	6.623	13.956	12.754	13.223
Boiling point	−12.338	1.043	4.684	3.032	0.337
Vapor pressure	−9.139	0.627	4.394	2.742	2.753
Deformation polarizability	6.616	4.298	3.751	3.075	10.626
Topological index	22.060	11.039	−0.453	0.397	7.628
DHvap	−7.843	0.847	6.179	5.118	2.673
Global average	10.310	4.600	5.539	6.133	8.663
h-BN surface					
Model or method	**CH_2Cl_2**	**Chloroform**	**THF**	**Ethyl acetate**	**Acetone**
Kiselev	7.838	−3.675	3.246	6.286	15.141
Cylindric	21.366	19.028	0.042	6.187	8.332
Van der Waals	12.103	7.096	11.756	10.101	17.662
Redlich-Kwong	12.296	7.218	11.890	10.193	17.772
Geomeric	18.720	16.644	4.728	8.120	9.345
Spheric	13.858	3.004	11.928	13.700	21.860
Hamieh model	6.162	0.311	8.752	11.671	8.376
Boiling point	11.142	12.753	5.590	1.030	4.887
Vapor pressure	7.717	13.456	5.973	1.832	2.320
Deformation polarizability	3.778	19.451	16.102	8.651	18.526
Topological index	23.279	27.710	10.925	5.351	14.827
DHvap	5.813	13.107	3.884	−1.427	2.168
Global average	12.006	11.342	7.901	6.808	11.768

Table 4. Variations of $(-\Delta S_a^{sp} in\ J\ K^{-1}mol^{-1})$ as a function of the used models or methods of the adsorbed polar molecules respectively on BPO_4 and h-BN materials.

BPO_4 surface					
Model or method	**CH_2Cl_2**	**Chloroform**	**THF**	**Ethyl acetate**	**Acetone**
Kiselev	18.3	59	22.5	−1.9	−13
Cylindric	−44.9	8.6	27.8	−0.9	−1.6
Van der Waals	26.5	−37.3	−7.6	8.9	18.5
Redlich-Kwong	26.9	−37	−7.2	9.2	18.8
Geomeric	41.1	−3.8	−20.4	2.2	2
Spheric	28.1	−50.2	−6.9	16.2	26.8
Hamieh model	7.0	9.0	24.0	20.0	25.0
Boiling point	−29.5	6.1	20.3	12.4	8.3
Vapor pressure	21.2	6.3	18.6	15.8	14.7
Deformation polarizability	19.9	1.9	−7.6	−3.3	8.2
Topological index	44.1	12.1	−14	−7.4	3.6
DHvap	−22.4	5.9	22.7	15.8	12.1
Global average	11.4	−1.6	6.0	7.3	10.3
h-BN surface					
Model or method	**CH_2Cl_2**	**Chloroform**	**THF**	**Ethyl acetate**	**Acetone**
Kiselev	19.7	−15.8	12.3	17.7	38.3
Cylindric	51.2	42.1	5.7	16.7	23.9
Van der Waals	28.8	9.3	30.2	25.8	44.0
Redlich-Kwong	29.2	9.5	30.5	26.0	44.2
Geomeric	46.2	44.6	15.1	19.2	25.0
Spheric	31.6	4.3	31.1	34.6	54.1
Hamieh model	6.6	2.8	9.7	15.6	10.9
Boiling point	30.9	39.8	15.4	1.7	12.8
Vapor pressure	21.9	40.4	17.4	0.0	6.0
Deformation polarizability	18.2	51.3	33.5	14.8	36.3
Topological index	51.7	65.5	24.6	9.1	29.9
DHvap	21.7	40.4	12.5	−2.6	8.1
Global average	29.8	27.9	19.8	14.9	27.8

The Lewis acid base parameters of BPO_4 and h-BN were obtained by drawing the values of $\left(\frac{-\Delta H_a^{sp}}{AN'}\right)$ and $\left(\frac{-\Delta S_a^{sp}}{AN'}\right)$ as a function of $\left(\frac{DN'}{AN'}\right)$ for all previous methods **(Figures 3** and **4**).

The linearity showed in **Figures 3** and **4** is insured for the several of the applied models and methods. The obtained values of the various acid base constants K_A, K_D, ω_A and ω_D for the all IGC methods are shown in **Table 5**, included the values obtained by taking the average of these IGC methods.

The results of **Table 5** clearly showed that the classical methods and models cannot be taken into consideration because of the small linear regression coefficient $\boldsymbol{R^2}$ that sometimes reaches 0.000 to 0.700, thus proving that there is no correlation (cylindric, VDW, Redlich-Kwong spheric, geometric, topological index models for BPO_4, and Kiselev, boiling point, geometric, vapor pressure, topological index and enthalpy of vaporization models for h-BN). For other models, one obtained negative values indicating the non-validity of such models (cylindric, boiling point, geometric, vapor pressure, topological index, spheric, boiling point and enthalpy of vaporization models for BPO_4, and cylindric model for h-BN). Only the thermal model gave the more precise results with the highest linear regression coefficient $\boldsymbol{R^2}$ equal to 1.000 for BPO_4 and 0.989 for h-BN. On **Table 6**, we resumed the results obtained by using the thermal model.

Table 6 proved that BPO_4 material exhibits an amphoteric surface, whereas, h-BN is twice more basic than acidic. By comparison with other studies in literature such as that of Isik *et al*.[40], we observed that the results are closer in the two studies for BPO_4 material with a deviation of 20% from the thermal model and they are too far from each other. The error committed by Isik *et al*.[40] exceeds 250%. This large deviation resulted from the use by these authors of Schultz method[5] that was proved in many previous studies[30–33] to be wrong.

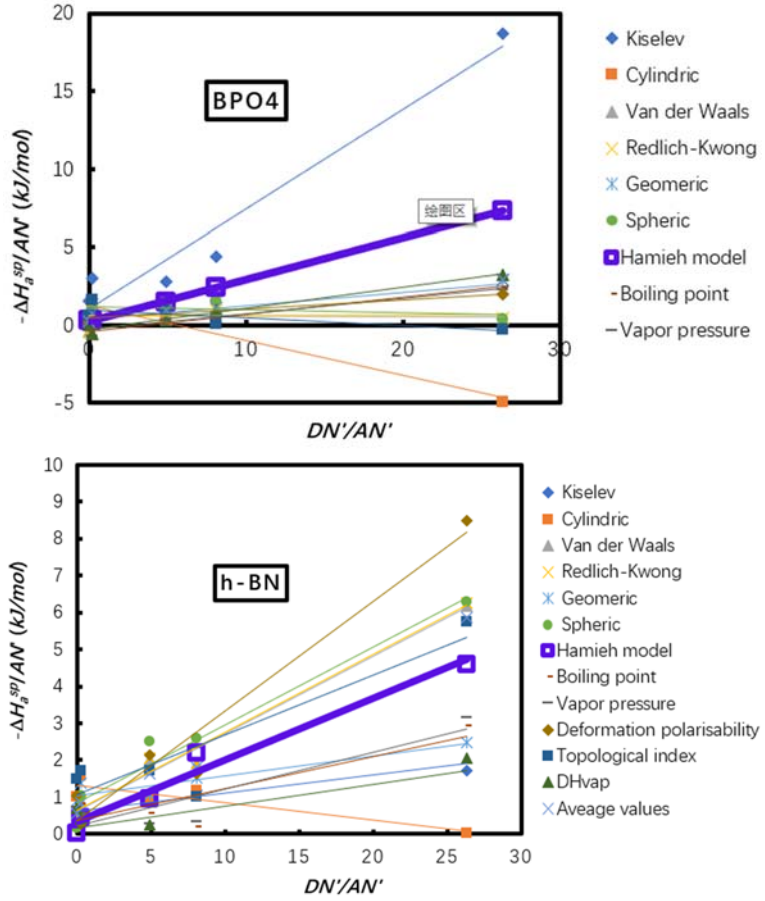

Figure 3. Variations of $\left(\frac{-\Delta H_a^{sp}}{AN'}\right)$ as a function of $\left(\frac{DN'}{AN'}\right)$ for different molecular models and IGC methods for the two analyzed boron materials.

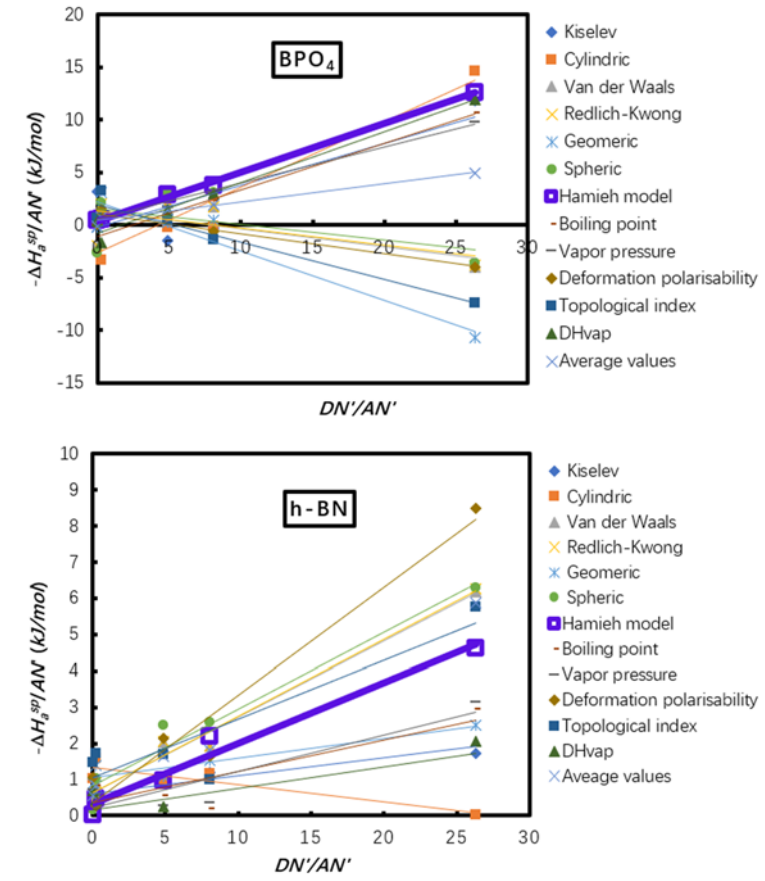

Figure 4. Variations of $\left(\frac{-\Delta S_a^{sp}}{AN'}\right)$ as a function of $\left(\frac{DN'}{AN'}\right)$ for different molecular models and IGC methods for h-BN and BPO_4 materials.

Table 5. Values of the enthalpic acid base constants K_A and K_D and the entropic acid base constants ω_A and ω_D of h-BN and BPO_4 for the various molecular models and IGC methods and the corresponding acid base ratios and the linear regression coefficients.

BPO_4						
Models and IGC methods	K_A	K_D	K_A/K_D	$10^{-3}\omega_A$	$10^{-3}\omega_D$	ω_D/ω_A
Kiselev	0.38	0.62	1.6	0.238	−0.15	-
Cylindric	−0.13	0.74	−5.6	0.37	−1.57	−4.2
Van der Waals	0.00	0.39	-	−0.10	0.77	-
Redlich-Kwong	0.00	0.39	-	−0.10	0.77	-
Geomeric	0.05	0.23	-	−0.28	1.35	−4.8
Spheric	−0.01	0.73	-	−0.09	0.93	-
Hamieh model	0.16	0.16	1.0	0.28	0.24	0.9
Boiling point	0.07	−0.26	−3.9	0.27	−0.65	−2.4
Vapor pressure	0.06	−0.17	−2.9	0.20	0.34	1.7
Deformation polarizability	0.03	0.26	7.6	−0.11	0.64	−5.7
Topological index	−0.03	0.59	-	−0.21	1.15	−5.4
Enthalpy of vaporization	0.08	−0.16	−2.0	0.29	−0.49	−1.7
Average values	0.05	0.29	-	0.06	0.28	-
h-BN						
Models and IGC methods	K_A	K_D	K_A/K_D	ω_A	ω_D	ω_D/ω_A
Kiselev	0.03	0.36	-	0.13	0.75	5.76
Cylindric	−0.03	0.79	-	0.00	1.78	-
Van der Waals	0.13	0.37	3.0	0.33	0.81	2.46
Redlich-Kwong	0.13	0.38	3.0	0.33	0.81	2.45
Geomeric	0.03	0.63	-	0.12	1.48	-
Spheric	0.13	0.50	4.0	0.34	1.13	3.37
Hamieh model	0.10	0.19	1.9	0.11	0.33	2.98
Boiling point	0.05	0.21	4.1	0.14	0.60	4.27
Vapor pressure	0.06	0.13	2.2	0.17	0.25	1.44
Deformation polarizability	0.18	0.22	1.2	0.36	0.61	1.70
Topological index	0.10	0.63	6.5	0.22	1.32	-
Enthalpy of vaporization	0.04	0.10	2.7	0.11	0.40	3.50
Average values	0.08	0.38	-	0.20	0.85	-

Table 6. Values of K_A, K_D, ω_A and ω_D for h-BN and BPO_4 with the acid base ratios and the linear regression coefficient by using Hamieh model.

Solid surface	K_A	K_D	K_A/K_D	R^2	$10^{-3}\omega_A$	$10^{-3}\omega_D$	ω_D/ω_A	R^2
BPO_4	0.16	0.16	1.0	1.000	0.28	0.24	0.9	0.998
h-BN	0.10	0.19	1.9	0.989	0.11	0.33	2.98	0.934

4. Conclusion

The inverse gas chromatography at infinite dilution was used to characterize the surface properties of h-BN and BPO_4 solid surfaces. Eight molecular models were applied to do that as well as five IGC methods. The dispersive components of the surface energy of h-BN and BPO_4 were calculated by the various molecular models. The results that took into account the thermal effect, were obtained by Hamieh model. The equations of $\gamma_s^d(T)$ of the two boron compounds were determined with an excellent accuracy. h-BN material exhibits a dispersive surface energy higher that BPO_4 surface, due to the difference in the surface and structural properties of these solid substrates. The entropic dispersive energy ε_s^d and T_{Max} present comparable values for the two boron surfaces.

The determination of the free surface energy led to obtain the values of specific free enthalpy ΔG_a^{sp}, from which we deduced the enthalpy and entropy of the different polar solvents adsorbed on the boron compounds by using 13 molecular models and chromatographic methods. The only valid model was that based on the thermal agitation taking into account the effect of the temperature. Our results proved that the boron materials have stronger specific interactions with the amphoteric organic solvents, due to the amphoteric character of these solid substrates. The values of the enthalpic acid base constants K_A and K_D and entropic acid base parameters ω_A *and* ω_D of the two boron materials were also determined and showed that BPO_4 has an amphoteric surface, whereas, h-BN exhibits a stronger basic character twice more basic than acidic. The tendency observed by Isik *et al.*[40] was the same as our above results but quantitatively

their results were wrong.

Funding

This research received no external funding.

Conflict of interest

The author declares no conflict of interest.

References

1. Conder JR, Young CL. Physical measurements by gas chromatography. Hoboken, New Jersey: Wiley; 1979.
2. Sawyer DT, Brookman DJ. Thermodynamically based gas chromatographic retention index for organic molecules using salt-modified aluminas and porous silica beads. Analytical Chemistry 1968; 40(12): 1847–1853. doi: 10.1021/ac60268a015.
3. Saint-Flour C, Papirer E. Gas-solid chromatography. A method of measuring surface free energy characteristics of short glass fibers. 1. Through adsorption isotherms. Industrial & Engineering Chemistry Product Research and Development 1982; 21(2): 337–341. doi: 10.1021/i300006a029.
4. Saint-Flour C, Papirer E. Gas-solid chromatography: method of measuring surface free energy characteristics of short fibers. 2. Through retention volumes measured near zero surface coverage. Industrial & Engineering Chemistry Product Research and Development 1982; 21(4): 666–669. doi: 10.1021/i300008a031.
5. Schultz J, Lavielle L, Martin C. The role of the interface in carbon fibre-epoxy composites. The Journal of Adhesion 1987; 23(1): 45–60. doi: 10.1080/00218468708080469.
6. Balard H, Sidqi M, Papirer E, *et al*. Study of modified silicas by inverse gas chromatography part II: Influence of chain length on surface properties of silicas grafted with α–ω diols. Chromatographia 1988; 25: 712–716. doi: 10.1007/BF02290477.
7. Sidqi M, Ligner G, Jagiello J, *et al*. Characterization of specific interaction capacity of solid surfaces by adsorption of alkanes and alkenes. Part I: Adsorption on open surfaces. Chromatographia 1989; 28: 588–592. doi: 10.1007/BF02260683.
8. Sidqi M, Balard H, Papirer E, *et al*. Study of modified silicas by inverse gas chromatography. Influence of chain length on the conformation of n-alcohols grafted on a pyrogenic silica. Chromatographia 1989; 27: 311–315. doi: 10.1007/BF02321275.
9. Balard H, Sidqi M, Papirer E, *et al*. Study of modified silicas by inverse gas chromatography. Part I: Influence of chain length on grafting ratio. Chromatographia 1988; 25: 707–711. doi: 10.1007/BF02290476.
10. Papirer E, Brendlé E, Balard H, Dentzer J. Variation of the surface properties of nickel oxide upon heat treatment evidenced by temperature programmed desorption and inverse gas chromatography studies. Journal of Materials Science 2000; 35: 3573–3577. doi: 10.1023/A:1004813629876.
11. Donnet JB, Ridaoui H, Balard H, *et al*. Evolution of the surface polar character of pyrogenic silicas, with their grafting ratios by dimethylchlorosilane, studied by microcalorimetry. Journal of Colloid and Interface Science 2008; 325(1): 101–106. doi: 10.1016/j.jcis.2008.05.025.
12. Przybyszewska M, Krzywania A, Zaborski M, Szynkowska MI. Surface properties of zinc oxide nanoparticles studied by inverse gas chromatography. Journal of Chromatography A 2009; 1216(27): 5284–5291. doi: 10.1016/j.chroma.2009.04.094.
13. Bakaoukas N, Sevastos D, Kapolos J, *et al*. Characterization of polymeric coatings in terms of their ability to protect marbles and clays against corrosion from sulfur dioxide by inverse gas chromatography. International Journal of Polymer Analysis and Characterization 2013; 18(6): 401–413. doi: 10.1080/1023666X.2013.785647.
14. Brendlé E, Papirer E. A new topological index for molecular probes used in inverse gas chromatography for the surface nanorugosity evaluation. Journal of Colloid and Interface Science 1997; 194(1): 207–216. doi: 10.1006/jcis.1997.5104.
15. Rückriem M, Inayat A, Enke D, *et al*. Inverse gas chromatography for determining the dispersive surface energy of porous silica. Colloids and Surfaces A: Physicochemical and Engineering Aspects 2010; 357(1–3): 21–26. doi: 10.1016/j.colsurfa.2009.12.001.
16. Boudriche L, Chamayou A, Calvet R, *et al*. Influence of different dry milling processes on the properties of an attapulgite clay, contribution of inverse gas chromatography. Powder Technology 2014; 254: 352–363. doi: 10.1016/j.powtec.2014.01.041.
17. Demertzis P, Riganakos K, Kontominas M. Water sorption isotherms of crystalline raffinose by inverse gas chromatography. International Journal of Food Science & Technology 1989; 24(6): 629–636. doi: 10.1111/j.1365-2621.1989.tb00689.x.
18. Helen H, Gilbert S. Moisture sorption of dry bakery products by inverse gas chromatography. Journal of Food Science 1985; 50(2): 454–458. doi: 10.1111/j.1365-2621.1985.tb13426.x.

19. Apte S. Excipient-API interactions in dry powder inhalers. Journal of Excipients and Food Chemicals 2012; 3(4): 129–142.
20. Apostolopoulos D, Gilbert SG. Water sorption of coffee solubles by frontal inverse gas chromatography: Thermodynamic considerations. Journal of Food Science 1990; 55(2): 475–487. doi: 10.1111/j.1365-2621.1990.tb06790.x.
21. Basivi PK, Pasupuleti VR, Seella R, *et al*. Inverse gas chromatography study on London dispersive surface free energy and electron acceptor-donor of fluconazole drug. Journal of Chemical & Engineering Data 2017; 62(7): 2090–2094. doi: 10.1021/acs.jced.7b00169.
22. Jones MD, Young P, Traini D. The use of inverse gas chromatography for the study of lactose and pharmaceutical materials used in dry powder inhalers. Advanced Drug Delivery Reviews 2012; 64(3): 285–293. doi: 10.1016/j.addr.2011.12.015.
23. Hamieh T, Rezzaki M, Schultz J. Study of the second order transitions and acid-base properties of polymers adsorbed on oxides by using inverse gas chromatography at infinite dilution: I. theory and methods. Journal of Colloid and Interface Science 2001; 233(2): 339–342. doi: 10.1006/jcis.2000.7267.
24. Hamieh T, Schultz J. New approach to characterise physicochemical properties of solid substrates by inverse gas chromatography at infinite dilution. I. Some new methods to determine the surface areas of some molecules adsorbed on solid surfaces. Journal of Chromatography A 2002; 969(1–2): 17–25. doi: 10.1016/S0021-9673(02)00368-0.
25. Hamieh T, Schultz J. New approach to characterise physicochemical properties of solid substrates by inverse gas chromatography at infinite dilution: II. Study of the transition temperatures of poly(methyl methacrylate) at various tacticities and of poly(methyl methacrylate) adsorbed on alumina and silica. Journal of Chromatography A 2002; 969(1–2): 27–36. doi: 10.1016/S0021-9673(02)00358-8.
26. Hamieh T. Fadlallah MB, Schultz J. New approach to characterise physicochemical properties of solid substrates by inverse gas chromatography at infinite dilution: III. Determination of the acid-base properties of some solid substrates (polymers, oxides and carbon fibres): A new model. Journal of Chromatography A 2002; 969(1–2): 37–47. doi: 10.1016/S0021-9673(02)00369-2.
27. Hamieh T, Schultz J. Inverse gas chromatography study of the influence of temperature on the surface area of adsorbed molecules (French). Journal de Chimie Physique 1996; 93: 1292–1331. doi: 10.1051/jcp/1996931292.
28. Hamieh T, Schultz J. Study of the adsorption of n-alkanes on polyethylene surface. State equations, molecule areas and fraction of surface covered. Comptes Rendus de l'Académie des Sciences, Série IIb 1996; 323(4): 281–289.
29. Hamieh T, Schultz J. A new method of calculation of polar molecule area adsorbed on MgO and ZnO by inverse gas chromatography. Comptes Rendus de l'Académie des Sciences, Série IIb 1996; 322(8): 627–633.
30. Hamieh T. Study of the temperature effect on the surface area of model organic molecules, the dispersive surface energy and the surface properties of solids by inverse gas chromatography. Journal of Chromatography A 2020; 1627: 461372. doi: 10.1016/j.chroma.2020.461372.
31. Hamieh T, Ahmad AA, Roques-Carmes T, Toufaily J. New approach to determine the surface and interface thermodynamic properties of H-β-zeolite/rhodium catalysts by inverse gas chromatography at infinite dilution. Scientific Reports 2020; 10(1): 1–27. doi: 10.1038/s41598-020-78071-1.
32. Hamieh T. New methodology to study the dispersive component of the surface energy and acid-base properties of silica particles by inverse gas chromatography at infinite dilution. Journal of Chromatographic Science 2022; 60(2): 126–142. doi: 10.1093/chromsci/bmab066.
33. Hamieh T. New physicochemical methodology for the determination of the surface thermodynamic properties of solid particles. AppliedChem 2023; 3(2): 229–255. doi: 10.3390/appliedchem3020015.
34. Chehimi MM, Abel ML, Perruchot C, *et al*. The determination of the surface energy of conducting polymers by inverse gas chromatography at infinite dilution. Synthetic Metals 1999; 104(1): 51–59. doi: 10.1016/S0379-6779(99)00040-5.
35. Peng Y, Gardner DJ, Han Y, *et al*. Influence of drying method on the surface energy of cellulose nanofibrils determined by inverse gas chromatography. Journal of Colloid and Interface Science 2013; 405: 85–95. doi: 10.1016/j.jcis.2013.05.033.
36. Puig C, Meijer H, Michels M, *et al*. Characterization of glass transition temperature and surface energy of bituminous binders by inverse gas chromatography. Energy & Fuels 2004; 18(1): 63–67. doi: 10.1021/ef0300621.
37. Mohammadi-Jam S, Burnett DJ, Waters KE. Surface energy of minerals-Applications to flotation. Minerals Engineering 2014; 66: 112–118. doi: 10.1016/j.mineng.2014.05.002.
38. Shui M, Reng Y, Pu B, Li J. Variation of surface

characteristics of silica-coated calcium carbonate. Journal of Colloid and Interface Science 2004; 273(1): 205–210. doi: 10.1016/j.jcis.2004.01.018.
39. Bandosz TJ, Putyera K, Jagiełło J, Schwarz JA. Application of inverse gas chromatography to the study of the surface properties of modified layered minerals. Microporous Materials 1993; 1(1): 73–79. doi: 10.1016/0927-6513(93)80010-R.
40. Isik B, Ugraskan V, Cakar F, Yazici O. Investigation of the surface properties of hexagonal boron nitride and boron phosphate by inverse gas chromatography at infinite dilution. Journal of Chromatographic Science 2023; 61(1): 7–14. doi: 10.1093/chromsci/bmac017.
41. Dorris GM, Gray DG. Adsorption of n-alkanes at zero surface coverage on cellulose paper and wood fibers. Journal of Colloid and Interface Science 1980; 77(2): 353–362. doi: 10.1016/0021-9797(80)90304-5.
42. Fowkes FM. Interface acid-base/charge-transfer properties. In: Andrade JD (editor). Surface and interfacial aspects of biomedical polymers. New York: Springer New York; 1985. p. 337–372. doi: 10.1007/978-1-4684-8610-0_9.
43. Donnet JB, Park SJ, Balard H. Evaluation of specific interactions of solid surfaces by inverse gas chromatography. Chromatographia 1991; 31: 434–440. doi: 10.1007/BF02262385.
44. Chehimi MM, Pigois-Landureau E. Determination of acid–base properties of solid materials by inverse gas chromatography at infinite dilution. A novel empirical method based on the dispersive contribution to the heat of vaporization of probes. Journal of Materials Chemistry 1994; 4(5): 741–745. doi: 10.1039/JM9940400741.
45. Brendlé E, Papirer E. A new topological index for molecular probes used in inverse gas chromatography for the surface nanorugosity evaluation. Journal of Colloid and Interface Science 1997; 194(1): 207–216. doi: 10.1006/jcis.1997.5104.
46. Balard H, Brendlé E, Papirer E. Determination of the acid–base properties of solid surfaces using inverse gas chromatography: Advantages and limitations. In: Mittal KL (editor). Acid-base interactions, relevance to adhesion science and technology. Boca Raton: CRC Press; 2000. p. 299–316.
47. Gutmann V. The Donor-acceptor approach to molecular interactions. New York: Plenum Press; 1978.

Appendix

Table A1. Values of ($\Delta G_a^{sp}(T)$) (in kJ/mol) of the various polar solvents adsorbed on BPO4 material against the temperature by using the various models and IGC.

DGasp (T) (in kJ/mol)	**Kiselev**				
T (K)	**CH_2Cl_2**	**$CHCl_3$**	**THF**	**Ethyl acetate**	**Acetone**
303.15	3.454	1.206	0.157	1.103	4.497
308.15	3.360	1.484	0.270	1.095	4.434
313.15	3.267	1.769	0.382	1.085	4.369
318.15	3.175	2.062	0.494	1.076	4.304
323.15	3.085	2.367	0.607	1.067	4.239
328.15	2.996	2.682	0.719	1.057	4.173
DGasp (T) (in kJ/mol)	**Cylindrical**				
T (K)	**CH_2Cl_2**	**$CHCl_3$**	**THF**	**Ethyl acetate**	**Acetone**
303.15	7.106	5.924	-0.925	1.278	2.244
308.15	6.881	5.959	-0.786	1.275	2.237
313.15	6.655	5.996	-0.648	1.270	2.229
318.15	6.431	6.039	-0.508	1.266	2.221
323.15	6.208	6.087	-0.369	1.261	2.213
328.15	5.984	6.140	-0.231	1.256	2.204
DGasp (T) (in kJ/mol)	**VDW**				
T (K)	**CH_2Cl_2**	**$CHCl_3$**	**THF**	**Ethyl acetate**	**Acetone**
303.15	4.856	4.125	3.004	2.355	5.257
308.15	4.721	4.297	3.042	2.311	5.164
313.15	4.587	4.475	3.080	2.266	5.072
318.15	4.454	4.660	3.118	2.221	4.979
323.15	4.324	4.854	3.156	2.177	4.887
328.15	4.194	5.058	3.194	2.132	4.794
DGasp (T) (in kJ/mol)	**R-K**				
T (K)	**CH_2Cl_2**	**$CHCl_3$**	**THF**	**Ethyl acetate**	**Acetone**
303.15	4.922	4.176	3.051	2.385	5.292
308.15	4.785	4.347	3.087	2.339	5.199
313.15	4.649	4.524	3.123	2.293	5.104
318.15	4.515	4.708	3.160	2.248	5.011
323.15	4.381	4.900	3.196	2.201	4.916
328.15	4.250	5.103	3.232	2.155	4.822
DGasp (T) (in kJ/mol)	**Geometric**				
T (K)	**CH_2Cl_2**	**$CHCl_3$**	**THF**	**Ethyl acetate**	**Acetone**
303.15	6.048	3.013	0.747	2.364	2.874
308.15	5.842	3.031	0.849	2.354	2.864
313.15	5.637	3.049	0.951	2.343	2.854
318.15	5.431	3.068	1.053	2.332	2.844
323.15	5.226	3.088	1.155	2.320	2.834
328.15	5.022	3.109	1.257	2.308	2.823
DGasp (T) (in kJ/mol)	**Spherical**				
T (K)	**CH_2Cl_2**	**$CHCl_3$**	**THF**	**Ethyl acetate**	**Acetone**
303.15	5.681	4.122	2.911	3.209	6.277
308.15	5.538	4.357	2.945	3.127	6.143
313.15	5.396	4.598	2.980	3.045	6.008
318.15	5.256	4.848	3.015	2.964	5.874
323.15	5.117	5.108	3.049	2.883	5.740
328.15	4.980	5.379	3.084	2.803	5.607
DGasp (T) (in kJ/mol)	**Hamieh model**				
T (K)	**CH_2Cl_2**	**$CHCl_3$**	**THF**	**Ethyl acetate**	**Acetone**
303.15	1.878	3.895	6.680	6.691	5.644
308.15	1.843	3.850	6.560	6.591	5.519
313.15	1.808	3.805	6.440	6.491	5.394
318.15	1.773	3.760	6.320	6.391	5.269
323.15	1.738	3.715	6.200	6.291	5.144
328.15	1.703	3.670	6.080	6.191	5.019

Table A1. (*Continued*).

DGasp (T) (in kJ/mol)	Boiling point				
T (K)	**CH_2Cl_2**	**$CHCl_3$**	**THF**	**Ethyl acetate**	**Acetone**
303.15	3.384	0.805	1.456	0.740	2.180
308.15	3.236	0.835	1.557	0.802	2.221
313.15	3.088	0.865	1.658	0.864	2.262
318.15	2.941	0.897	1.760	0.927	2.304
323.15	2.793	0.927	1.861	0.989	2.346
328.15	2.646	0.957	1.962	1.051	2.387
DGasp (T) (in kJ/mol)	**Vapor pressure**				
T (K)	**CH_2Cl_2**	**$CHCl_3$**	**THF**	**Ethyl acetate**	**Acetone**
303.15	2.720	1.273	1.257	2.040	1.714
308.15	2.616	1.305	1.350	2.121	1.788
313.15	2.511	1.337	1.443	2.201	1.862
318.15	2.405	1.369	1.537	2.280	1.936
323.15	2.298	1.399	1.630	2.357	2.009
328.15	2.190	1.430	1.723	2.434	2.082
DGasp (T) (in kJ/mol)	**Deformation polarizability**				
T (K)	**CH_2Cl_2**	**$CHCl_3$**	**THF**	**Ethyl acetate**	**Acetone**
303.15	0.146	3.737	6.060	4.078	8.154
308.15	0.048	3.728	6.098	4.095	8.114
313.15	–0.052	3.719	6.136	4.111	8.073
318.15	–0.151	3.709	6.174	4.127	8.032
323.15	–0.251	3.700	6.212	4.144	7.991
328.15	–0.349	3.691	6.251	4.161	7.951
DGasp (T) (in kJ/mol)	**Topological index**				
T (K)	**CH_2Cl_2**	**$CHCl_3$**	**THF**	**Ethyl acetate**	**Acetone**
303.15	8.706	7.366	3.796	2.636	6.539
308.15	8.485	7.305	3.865	2.672	6.520
313.15	8.265	7.245	3.935	2.710	6.503
318.15	8.044	7.184	4.005	2.746	6.484
323.15	7.825	7.123	4.075	2.783	6.466
328.15	7.605	7.063	4.146	2.821	6.449
DGasp (T) (in kJ/mol)	**DHvap**				
T (K)	**CH_2Cl_2**	**$CHCl_3$**	**THF**	**Ethyl acetate**	**Acetone**
303.15	1.038	0.954	0.701	–0.343	0.980
308.15	0.926	0.984	0.815	–0.264	1.040
313.15	0.814	1.014	0.928	–0.185	1.101
318.15	0.702	1.044	1.042	–0.106	1.161
323.15	0.590	1.074	1.156	–0.027	1.221
328.15	0.477	1.102	1.268	0.051	1.281

Table A2. Values of ($\Delta G_a^{sp}(T)$) (in kJ/mol) of the various polar solvents adsorbed on h-BN material against the temperature by using the various models and IGC.

DGasp (T) (in kJ/mol)	Kiselev				
T (K)	**CH_2Cl_2**	**$CHCl_3$**	**THF**	**Ethyl acetate**	**Acetone**
303.15	1.881	1.142	–0.490	0.930	3.540
308.15	1.780	1.207	–0.552	0.840	3.347
313.15	1.681	1.278	–0.614	0.752	3.155
318.15	1.583	1.356	–0.675	0.663	2.964
323.15	1.486	1.443	–0.737	0.576	2.773
328.15	1.390	1.539	–0.798	0.488	2.583
DGasp (T) (in kJ/mol)	**Cylindrical**				
T (K)	**CH_2Cl_2**	**$CHCl_3$**	**THF**	**Ethyl acetate**	**Acetone**
303.15	3.378	4.296	2.591	2.275	4.335
308.15	3.230	4.236	2.438	2.143	4.112
313.15	3.084	4.182	2.286	2.013	3.891
318.15	2.939	4.133	2.134	1.882	3.670
323.15	2.800	4.097	1.987	1.758	3.454
328.15	2.657	4.064	1.835	1.629	3.235
DGasp (T) (in kJ/mol)	**VDW**				
T (K)	**CH_2Cl_2**	**$CHCl_3$**	**THF**	**Ethyl acetate**	**Acetone**
303.15	3.378	4.296	2.591	2.275	4.335
308.15	3.230	4.236	2.438	2.143	4.112
313.15	3.084	4.182	2.286	2.013	3.891

Table A2. (*Continued*).

DGasp (T) (in kJ/mol)	VDW				
T (K)	CH_2Cl_2	$CHCl_3$	THF	Ethyl acetate	Acetone
318.15	2.939	4.133	2.134	1.882	3.670
323.15	2.800	4.097	1.987	1.758	3.454
328.15	2.657	4.064	1.835	1.629	3.235
DGasp (T) (in kJ/mol)	**R-K**				
T (K)	**CH_2Cl_2**	**$CHCl_3$**	**THF**	**Ethyl acetate**	**Acetone**
303.15	3.449	4.351	2.641	2.306	4.372
308.15	3.300	4.291	2.487	2.174	4.149
313.15	3.153	4.236	2.335	2.044	3.928
318.15	3.008	4.189	2.183	1.914	3.707
323.15	2.862	4.147	2.030	1.784	3.486
328.15	2.719	4.115	1.878	1.656	3.267
DGasp (T) (in kJ/mol)	**Geometric**				
T (K)	**CH_2Cl_2**	**$CHCl_3$**	**THF**	**Ethyl acetate**	**Acetone**
303.15	4.712	3.114	0.155	2.306	1.769
308.15	4.480	2.890	0.079	2.210	1.644
313.15	4.249	2.666	0.004	2.114	1.519
318.15	4.018	2.443	–0.072	2.018	1.394
323.15	3.787	2.220	–0.147	1.922	1.269
328.15	3.557	1.998	–0.223	1.827	1.144
DGasp (T) (in kJ/mol)	**Spherical**				
T (K)	**CH_2Cl_2**	**$CHCl_3$**	**THF**	**Ethyl acetate**	**Acetone**
303.15	4.294	4.309	2.502	3.216	5.463
308.15	4.134	4.317	2.346	3.040	5.190
313.15	3.974	4.330	2.189	2.865	4.918
318.15	3.817	4.350	2.034	2.692	4.648
323.15	3.660	4.379	1.880	2.521	4.379
328.15	3.505	4.417	1.725	2.351	4.111
DGasp (T) (in kJ/mol)	**Hamieh model**				
T (K)	**CH_2Cl_2**	**$CHCl_3$**	**THF**	**Ethyl acetate**	**Acetone**
303.15	4.190	0.500	5.811445	6.94186	5.074
308.15	4.137	0.545	5.762945	6.86386	5.005
313.15	4.095	0.575	5.714445	6.78586	4.944
318.15	4.062	0.588	5.665945	6.70786	4.889
323.15	4.039	0.587	5.617445	6.62986	4.841
328.15	4.026	0.569	5.568945	6.55186	4.800
DGasp (T) (in kJ/mol)	**Boiling point**				
T (K)	**CH_2Cl_2**	**$CHCl_3$**	**THF**	**Ethyl acetate**	**Acetone**
303.15	1.782	0.689	0.910	0.521	0.992
308.15	1.628	0.491	0.834	0.513	0.929
313.15	1.474	0.291	0.756	0.505	0.864
318.15	1.319	0.092	0.679	0.496	0.800
323.15	1.165	–0.107	0.602	0.488	0.735
328.15	1.010	–0.306	0.524	0.479	0.671
DGasp (T) (in kJ/mol)	**Vapor pressure**				
T (K)	**CH_2Cl_2**	**$CHCl_3$**	**THF**	**Ethyl acetate**	**Acetone**
303.15	1.079	1.213	0.709	1.950	0.502
308.15	0.972	1.013	0.622	1.956	0.473
313.15	0.863	0.810	0.534	1.958	0.442
318.15	0.754	0.609	0.448	1.961	0.413
323.15	0.643	0.406	0.361	1.961	0.382
328.15	0.532	0.204	0.275	1.960	0.352
DGasp (T) (in kJ/mol)	**Deformation polarizability**				
T (K)	**CH_2Cl_2**	**$CHCl_3$**	**THF**	**Ethyl acetate**	**Acetone**
303.15	–1.727	3.902	5.949	4.175	7.528
308.15	–1.819	3.645	5.781	4.100	7.346
313.15	–1.909	3.389	5.614	4.027	7.165
318.15	–1.999	3.133	5.446	3.953	6.984
323.15	–2.090	2.876	5.279	3.879	6.802
328.15	–2.181	2.620	5.111	3.805	6.621
DGasp (T) (in kJ/mol)	**Topological index**				
T (K)	**CH_2Cl_2**	**$CHCl_3$**	**THF**	**Ethyl acetate**	**Acetone**
303.15	7.609	7.860	3.478	2.601	5.765
308.15	7.350	7.532	3.355	2.555	5.615
313.15	7.092	7.205	3.233	2.510	5.466

Table A2. (*Continued*).

DGasp (T) (in kJ/mol)	Topological index				
T (K)	**CH_2Cl_2**	**$CHCl_3$**	**THF**	**Ethyl acetate**	**Acetone**
318.15	6.834	6.878	3.110	2.465	5.316
323.15	6.575	6.550	2.987	2.420	5.167
328.15	6.316	6.223	2.864	2.374	5.017
DGasp (T) (in kJ/mol)	**DHvap**				
T (K)	**CH_2Cl_2**	**$CHCl_3$**	**THF**	**Ethyl acetate**	**Acetone**
303.15	–0.757	0.864	0.101	–0.649	–0.301
308.15	–0.865	0.662	0.038	–0.636	–0.342
313.15	–0.974	0.460	–0.024	–0.624	–0.382
318.15	–1.082	0.258	–0.086	–0.611	–0.423
323.15	–1.191	0.056	–0.149	–0.598	–0.464
328.15	–1.299	–0.146	–0.211	–0.585	–0.504